

Plankton, Aerosol, Cloud, ocean Ecosystem (PACE) mission,

**The PACE Level 1c data format**  
**DRAFT 2021/09/28**



National Aeronautics and  
Space Administration

---

**Goddard Space Flight Center**  
**Greenbelt, Maryland**

---

## Table of Contents

1	INTRODUCTION .....	3
1.1	Purpose.....	3
1.2	Instrument Specifics.....	3
2	FILE NAME CONVENTION .....	5
3	PROJECTION .....	6
4	SPATIAL RESOLUTION AND SWATH.....	7
5	MULTI-VIEW AGGREGATION.....	7
6	DATA FIELDS.....	8
7	EXTERNAL DATA AND SOFTWARE.....	16
7.1	Re-aggregation tool.....	16
7.2	Downsampling tool.....	16
7.3	Ancillary and OCI derived data on the L1C grid.....	16
8	REFERENCES .....	16
9	APPENDIX A: ACRONYMS .....	18
10	APPENDIX B: SAMPLE CDL FOR HARP2.....	20
11	APPENDIX C: SAMPLE CDL FOR OCI .....	25
12	APPENDIX D: SAMPLE CDL FOR SPEXONE .....	29

## List of Figures

Figure 1	Expected L1C coverage for OCI (white), HARP2 (teal) and SPEXone (yellow).....	4
Figure 2	SOCEA Projection for an orbit track along the Prime Meridian. Cropped from: <a href="https://www.giss.nasa.gov/tools/gprojector/help/projections/">https://www.giss.nasa.gov/tools/gprojector/help/projections/</a> .....	6
Figure 3	Illustration of multi-view aggregation.....	8

## List of Tables

Table 1	Instrument characteristics .....	3
Table 2	Data dimensions for each instrument.....	9
Table 3	Global attributes.....	9
Table 4	SENSOR_VIEWS_BANDS group.....	10
Table 5	BIN_ATTRIBUTES group.....	10
Table 6	GEOLOCATION_DATA group .....	12
Table 7	OBSERVATION_DATA group.....	12

---

# 1 INTRODUCTION

## 1.1 Purpose

NASA's Plankton, Aerosol, Cloud, ocean Ecosystem (PACE) mission will make global ocean color and atmospheric measurements to provide extended data records of ocean ecology and global biogeochemistry, along with polarimetric measurements for advanced observations of aerosols, clouds and the ocean. PACE will contain three instruments: the primary Ocean Color Instrument (OCI), and two multi-angle polarimeters (MAPs). The latter instruments are contributed under a 'Do-No-Harm' (to the rest of the PACE mission) principle, and the PACE Science Data Processing System (SDPS) is only required to produce Level-1b (geolocated radiances with calibration applied) data without performance requirements. However, there is a strong desire to produce data in a format that merges the disparate spatial resolutions, viewing geometry and sampling nature of the three instruments. Our terminology for this format is Level 1c (L1C). This format will be an input to Level 2 algorithms produced from standalone MAP instrument observations, or from algorithms employing multi-sensor fusion.

Creating the L1C format has several components. This includes choice of projection method, the means by which multi-angle views are properly incorporated into that projection ('aggregation'), the selection of data to be included within the L1C file, and the handling of ancillary data either required for L1C file generation or needed in that format for L2 processing.

The guiding philosophy of the PACE L1C file format is to be a means to gather data from all instruments onto a common sampling grid. This grid will be equal area and contain observations for all instruments and viewing angles for a specified height.

PACE serves the needs of multiple disciplines, and as such there may exist various preferences for L1C format depending on the application. It may not be possible to satisfy all potential users, who may need to re-project or otherwise process L1C data depending on its usage.

The purpose of this document is therefore to describe the L1C file format to be universally applied for PACE. **Standard processing to L2 for all polarimeters shall accept as input this L1C product.**

## 1.2 Instrument Specifics

While detailed descriptions of the three PACE instruments can be found elsewhere (e.g. Werdell et al., 2019, Martins et al., 2018, Hasekamp et al., 2019, among others) we provide a brief description of the spectral, polarimetric and geometric aspects of each instrument in Table 1.

Table 1 Instrument characteristics

	<b>Ocean Color Instrument (OCI)</b>	<b>Hyper-Angular Rainbow Polarimeter 2 (HARP2)</b>	<b>Spectro-Polarimeter for Planetary Exploration one (SPEXone)</b>
--	-------------------------------------	--	--

UV-VIS radiance channels	<b>240</b> : continuous coverage in 340-890nm range at 2.5nm spectral resolution (5nm bandwidth)	<b>4</b> : 441, 549, 669, 873 nm	<b>~400</b> : continuous coverage in 385-770nm at 2-5nm spectral resolution
UV-VIS polarimetric channels	-	<b>4</b> : 441, 549, 669, 873 nm	<b>~50</b> : continuous coverage in 385-770nm at 10-40nm spectral resolution
SWIR radiance channels	<b>7</b> : 940, 1038, 1250, 1378, 1615, 2130, and 2260 nm	-	-
Viewing zenith angles at ground or top of atmosphere (TOA) for swath center	<b>1</b> : TOA 20° North in northern hemisphere, TOA 20° South in southern hemisphere to avoid ocean surface glint	<b>60</b> angles between ± 57° TOA along track for 669nm, <b>10</b> angles for the other bands*	<b>5</b> : 0°, ±20° and ±58° at ground
Nadir view, at-ground swath width	2663km <sup>@</sup>	1,556 km	100km
Spatial Resolution	1x1km at nadir <sup>@</sup>	TBD, but roughly 5km <sup>2</sup>	5.4 x 4.6 km <sup>#</sup> for all view angles

\*note that the set of viewing angles for HARP2 are slightly different for each spectral channel.

<sup>#</sup>the SPEXone spatial sampling is 2.6km<sup>2</sup>.

<sup>@</sup>Since OCI only views at 20° forward or aft, the OCI swath width is presented at that angle, and the spatial resolution at those angles are slightly larger.

The intent of the L1C format is to represent radiometric data observed by the three PACE instruments on a common grid. For grids with data from multiple instruments, this would facilitate their merged usage in a L1C to L2 algorithm. For example, OCI SWIR channels could provide coarse mode aerosol information for a SPEXone aerosol retrieval, or HARP2 multi-angle measurements could be used to perform a superior atmospheric correction for OCI. Potential uses for such combined datasets were explored by the first PACE Science Team, described in reviews such as Frouin et al., 2019 and Remer et al., 2019. Additionally, a L1C product could aid in easy instrument cross calibration or validation. Four types of files will be generated, one for each PACE instrument (OCI, HARP2 and SPEXone) and a fourth to contain

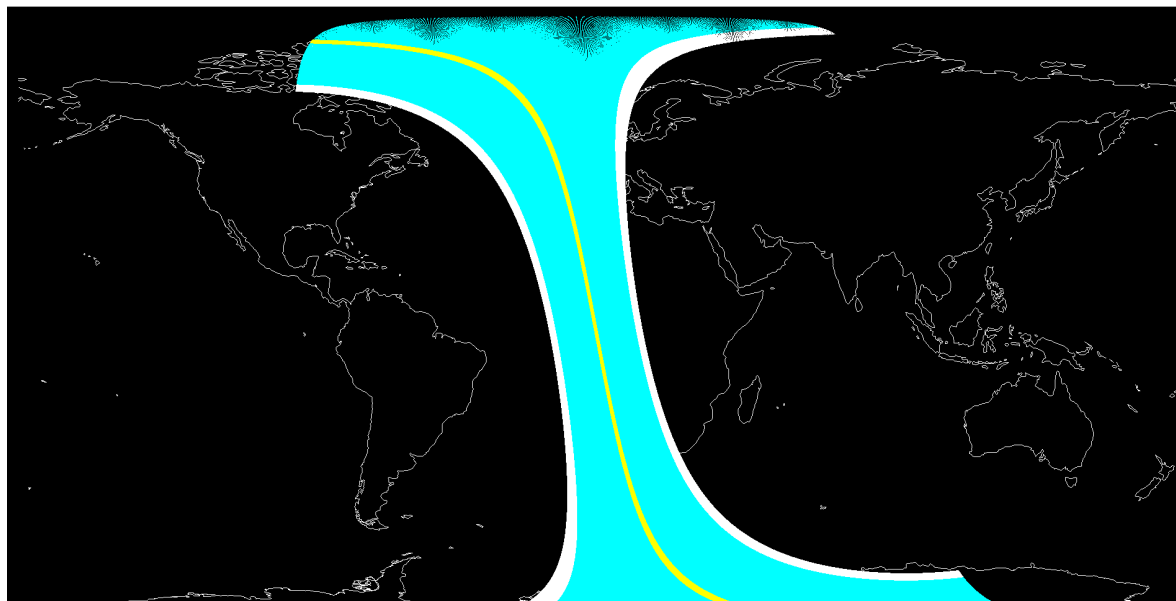


Figure 1 Expected L1C coverage for OCI (white), HARP2 (teal) and SPEXone (yellow).

ancillary data (such as OCI derived cloud flags, and MERRA-2 (Gelaro et al., 2017) reanalysis data). Due to varying spatial resolution, these files may have different grid sizes, but compatibility will be maintained by constraining these sizes to multiples of each other.

## 2 FILE NAME CONVENTION

The file naming convention of the Ocean Biology Processing Group (OBPG) and the Ocean Biology Distributed Active Archive Center (OB-DAAC), who will be performing the L1C data processing and archival, respectively, is described here:

<https://oceancolor.gsfc.nasa.gov/docs/filenaming-convention/>

### **MMMM\_III\_TTT.YYYYMMDDTHHMMSS.LLLL.PPPP.SSSS.pppp.RRRR.NRT.nc**

- **MMMM\***: variable-length uppercase character string indicating the "mission".
  - e.g. AQUA, PACE, S3A
- **III**: variable-length uppercase character string indicating the instrument
  - e.g. OCI (PACE Ocean Color Instrument)
- **TTT**: (value is absent if not relevant to product) variable-length uppercase character string indicating the data "type"
  - e.g. GAC (SeaWiFS Global Area Coverage); EFR (OLCI Full Resolution)
- **YYYYMMDDTHHMMSS**: ISO8601 time format, where YYYY is the 4-digit year, MM is the two-digit month, DD is the two-digit day, T indicates the time follows this character, HHMMSS are the two-digit hour, minutes, and seconds, respectively.
- **LLLL**: variable-length character string indicating the level.
  - e.g. L1B, L2, L3m
- **PPPP**: period indicator for L3
  - e.g. DAY, MO, YR, R32
- **SSSS**: suite identifier
  - e.g. RRS, CHL
- **pppp**: product identifier
  - e.g. Rrs\_412, chlor\_a
- **RRRR\*\***: resolution
  - e.g. 4km
- **NRT**: (value is absent if not relevant to product) Near Real-Time identifier. This location could also be used to identify a version number.

\* The mission identifier could be a reasonably shortened representation, e.g. Sentinel-3A = S3A

\*\* The resolution element includes the units, e.g. 4km, 1deg

Example filenames for January 15<sup>th</sup>, 2023 at 12:34:56 UTC would be:

```
PACE_OCI.20230115T123456.L1C.5.2km.V01.nc
PACE_HARP.20230115T123456.L1C.5.2km.V01.nc
PACE_SPEX.20230115T123456.L1C.2.6km.V01.nc
PACE_ANC.20230115T123456.L1C.2.6km.V01.nc
```

Note the PACE\_ANC\* files will contain ancillary data represented on the L1C grid. This could include assimilated meteorological data, cloud flags, or other external or derived information.

### 3 PROJECTION



Figure 2 SOCEA Projection for an orbit track along the Prime Meridian. Cropped from: <https://www.giss.nasa.gov/tools/gprojector/help/projections/>

The L1C format will use a swath-based Spacecraft Oblique Cylindrical Equal Area (SOCEA) projection (see Snyder, 1978 and 1987 for a description of the Oblique Cylindrical Equal Area projection). This projection will have the vertical centerline aligned with the subsatellite track, horizontal bin spacing representing equal distances transverse to the orbit track, and vertical spacing that preserves the equal area grid. Bins are indexed by row and column, and constructed so that the intersection of the ground track with the equator corresponds to the meeting point of four bins along the centerline of the projection.

Figure 2 shows a map of the SOCEA projection. A new projection is defined for each orbit, centered about the orbit path, which for the purposes of demonstration is the Prime Meridian in this figure.

Bin size uniformity is an important aspect of the L1C format projection. Ground spatial resolution is generally preserved for the SPEXone instrument, due to narrow swath and specially designed optics for fore and aft views intended for this purpose. This will not be the case, however, for OCI and HARP2. For those instruments, the ground spatial resolution will grow as the view zenith angle increases from nadir. This would be a problem for algorithms that utilize multiple views and instruments, as they are (almost universally) built on the assumption that all observations represent the same location. The SOCEA projection satisfies the requirement for equal area bins, the size of which are described in more detail in the next section.

In addition to the advantages described above, the SOCEA projection is easily viewed as stored. However, the specific projection must be defined for each orbit, and there is no inherent relationship between row/column and latitude/longitude, so the latter must also be stored for each bin.

Another advantage of this format is that users of L2 (geophysical) data are more likely to use a format which can be easily viewed as images, and it is simplest to maintain the projection and format in the

L1C to L2 processing. However, we should note the Level 3 binned products will likely use an integerized sinusoidal binning scheme (see: <https://oceancolor.gsfc.nasa.gov/docs/format/l3bins/>)

## 4 SPATIAL RESOLUTION AND SWATH

The ground spatial resolution for the OCI instrument is  $1\text{km}^2$  at nadir, the SPEXone ground sampling resolution is  $2.6\text{km}^2$ , while the HARP2 ground sampling resolution is TBD, pending optimization of onboard spacecraft binning to minimize downlink bandwidth. For OCI and HARP2, the spatial resolution will vary depending on along or cross track viewing angle. Of the four onboard binning modes under consideration for HARP2, the finest spatial resolution is  $3.6\text{km} \times 3.5\text{km}$  at viewing angle extremes, and the coarsest is  $7.2\text{km} \times 5.2\text{km}$ .

For these reasons, we intend to bin SPEXone data to an area equivalent to a  $2.6 \times 2.6 \text{ km}$  resolution and OCI to  $5.2\text{km}$ . For HARP2, we will use the smallest possible resolution that is a multiple of  $2.6\text{km}^2$ , depending on onboard binning scheme. Use of spatial resolution multiples will ensure that bin edges are aligned. This means that the number of bins in the across swath direction will be roughly 512 for OCI, 40 for SPEXone and TBD for HARP2. Data from the full swath for all instruments will be incorporated into the L1C format, including portions of the HARP2 swath that may not have nadir views due to broadening at the most forward and aft viewing angles.

The choice of the use of variable spatial resolutions is a tradeoff. On one hand, we would like to easily match coincident measurements from multiple instruments. On the other, we don't want to degrade an individual instrument's spatial resolution unnecessarily. We have therefore chosen a format that matches the geographic coordinates of the different instruments to a common grid, although in some cases the spacing of that grid for one instrument might be multiples of that of that for another. To assist the usage of multiple instrument datasets simultaneously, the NADIR\_BIN field is included that identifies the bin closest to nadir in each swath. Since the subsatellite track forms the boundary between two bins, the bin immediately to the east of this is what is identified by the NADIR\_BIN field. Additionally, a tool will be provided that can downsample and/or align data from multiple instruments to the same spatial resolution (see Section 7.2).

Data from the full instrument swath, for all three instruments, will be incorporated into L1C files. This will allow the L1C-L2 processing routines to decide the appropriate observation geometries to include.

The along track size of each file will be selected to optimize storage and single-core processing time feasibility. This precludes the use of files containing an entire orbit. While to some extent this complicates L1b to L1C processing (adjacent files may need to be used to aggregate multi-angle views for each bin), this is trivial once implemented in a systematic manner within a data processing system.

## 5 MULTI-VIEW AGGREGATION

The MAP instruments are designed to capture the angular dependence of scattering for a surface or volume of the atmosphere, which contains additional optical property information. L1C to L2 algorithms that utilize this information need the data organized so that it represents scattering about a single point. In practice, the multiple angle views are made as the spacecraft flies over that point, so the individual views have different sampling times. This means that the data are

organized in a L1b file in a manner that represents multi-angle views at the spacecraft altitude, not the geophysical point of interest. Thus, multi-angle views must be ‘aggregated’ to a specific ground location. Projection, as is described in Section 2, will achieve this purpose. It is a process that requires knowledge of the altitude of the bin location. Over the ocean, this altitude will by default be the ellipsoid surface. Over land, data will be aggregated to the altitude of a digital elevation model (DEM) at that location. Details of the specific DEM will be included in the file attributes, while the variability of elevations within a specific grid box will be stored in a data field. Currently, the DEM planned for use by PACE is the GEBCO\_2019 dataset ([https://www.gebco.net/data\\_and\\_products/gridded\\_bathymetry\\_data/gebco\\_2019/gebco\\_2019\\_info.html](https://www.gebco.net/data_and_products/gridded_bathymetry_data/gebco_2019/gebco_2019_info.html), doi:10.5285/836f016a-33be-6ddc-e053-6c86abc0788e), with minor modifications to report the height of a water body surface (not its bathymetry). Retrievals of cloud optical properties (or aerosols above clouds) will require re-aggregation to an alternative altitude. The L1C product produced for PACE will by default be the surface as described above, however, a software tool to re-aggregate to a given altitude will also be made available (see Section 7.1).

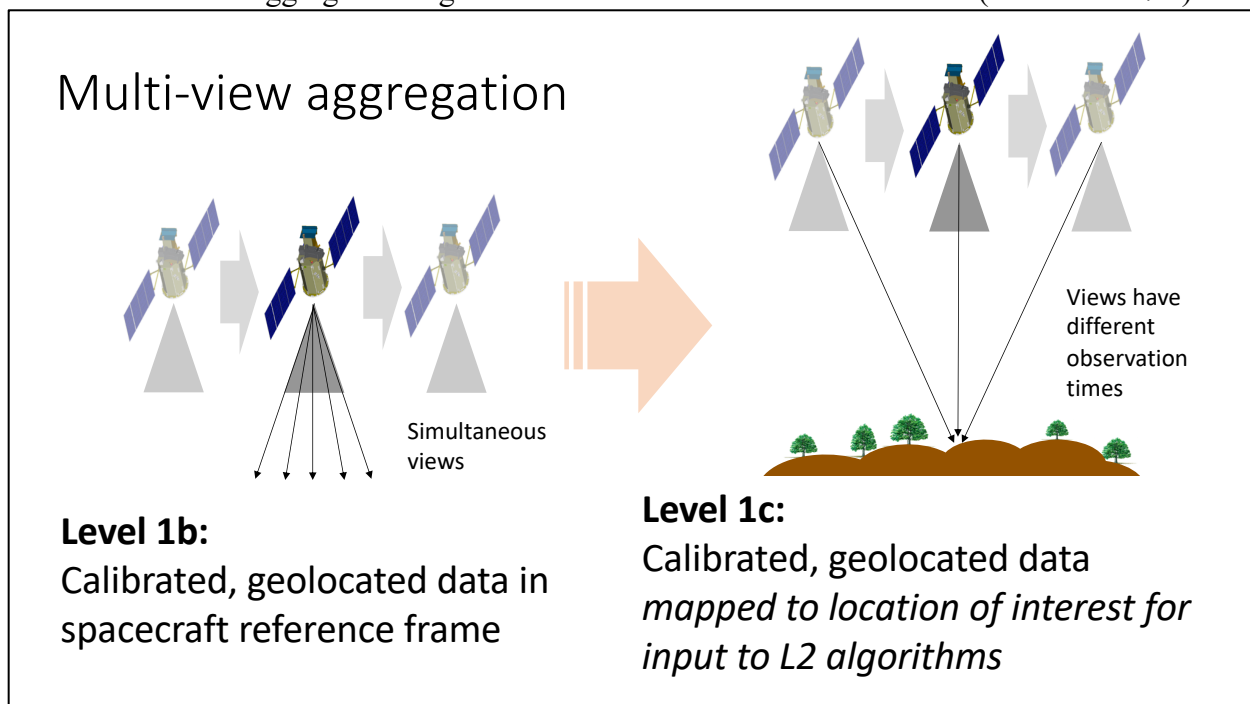


Figure 3 Illustration of multi-view aggregation

We note that multi-angle observations inherently contain information about feature altitude via parallax, and this can be used to determine cloud top (Moroney et al, 2002), cloud base (Böhm et al, 2019), aerosol plume altitude and wind speed (e.g. Nelson et al., 2013) or multiple cloud layers (Sinclair et al., 2017). Application of these techniques, if performed for PACE, will be a separate process than the L1b to L1C technique we describe here, but may inform the altitude used in a re-aggregation.

## 6 DATA FIELDS

The data fields for the L1C format are common for all instruments, although the dimensions may vary. Data are to be organized into four groups:

1. SENSOR\_VIEWS\_BANDS: contains information on viewing geometry, band center wavelengths and other information common to all bins,
2. BIN\_ATTRIBUTES: contains information specific to each bin,
3. GEOLOCATION\_DATA: contains latitude, longitude, altitude, observation and solar geometry,
4. OBSERVATION\_DATA: contains the data observed by the instrument.

These data groups will utilize five different dimensions, whose values will be different for each instrument. Table 2 is a description of these dimensions and potential values for each instrument

Table 2 Data dimensions for each instrument.

Dimension	OCI	HARP2	SPEXone
NUMBER OF VIEWS	2 <sup>a</sup>	90 <sup>b</sup>	5
INTENSITY BANDS PER VIEW	249	1	400
POLARIZATION BANDS PER VIEW	0	1	50
BINS ALONG TRACK	TBD	TBD	TBD
BINS ACROSS TRACK	512	TBD	40

Color is intended to aid cross reference to the data groups tables.

<sup>a</sup> OCI has a 20° fore or aft tilt depending on spacecraft hemisphere

<sup>b</sup> HARP2 will have 60 view angles for the channel centered at 669nm, 10 angles otherwise. Each channel will access unique viewing angles.

Table 3 contains global attributes that are required for the L1C format.

Table 3 Global attributes

Field	Description
TITLE	PACE [OCI/HARP/SPEX/ANC] Level-1c data
INSTRUMENT	[OCI/HARP/SPEX/ANC]
PROCESSING_VERSION	V1.0
CONVENTIONS	CF-1.6
INSTITUTION	NASA Goddard Space Flight Center, Ocean Biology Processing Group
LICENSE	<a href="http://science.nasa.gov/earth-science/earth-science-data/data-information-policy/">http://science.nasa.gov/earth-science/earth-science-data/data-information-policy/</a>
NAMING_AUTHORITY	<a href="http://gov.nasa.gsfc.sci.oceancolor">gov.nasa.gsfc.sci.oceancolor</a>
KEYWORD_VOCABULARY	NASA Global Change Master Directory (GCMD) Science Keywords
STDNAME_VOCABULARY	NetCDF Climate and Forecast (CF) Metadata Convention
CREATOR_NAME	NASA/GSFC
CREATOR_EMAIL	<a href="mailto:data@oceancolor.gsfc.nasa.gov">data@oceancolor.gsfc.nasa.gov</a>
CREATOR_URL	<a href="http://oceancolor.gsfc.nasa.gov">http://oceancolor.gsfc.nasa.gov</a>
PROJECT	PACE Project
PUBLISHER_NAME	NASA/GSFC
PUBLISHER_EMAIL	<a href="mailto:data@oceancolor.gsfc.nasa.gov">data@oceancolor.gsfc.nasa.gov</a>
PUBLISHER_URL	<a href="http://oceancolor.gsfc.nasa.gov">http://oceancolor.gsfc.nasa.gov</a>
PROCESSING_LEVEL	L1C
CDM_DATA_TYPE	swath
ORBIT_NUMBER	12345
HISTORY	
CDL version date	2020-02-20
PRODUCT_NAME	PACE [OCI/HARP/SPEX/ANC].20230115T123456.L1C.V01.nc
STARTDIRECTION	Ascending
ENDDIRECTION	Ascending
TIME_COVERAGE_START	yyyy-mm-ddThh:mm:ss.sssZ
TIME_COVERAGE_END	yyyy-mm-ddThh:mm:ss.sssZ
DATE_CREATED	yyyy-mm-ddThh:mm:ss.sssZ
SUN_EARTH_DISTANCE	1.0, Sun earth distance for data day of year, in AU
TERRAIN_DATA_SOURCE	Source of terrain data used for aggregation
SPECTRAL_RESPONSE_FUNCTION	Points to documentation containing this information
SYSTEMATIC_UNCERTAINTY_MODEL	Models (equations) for systematic uncertainty for I, DoLP, Q, U or q,u as relevant
NADIR_BIN	Cross track bin with view zenith angle closest to nadir. Since true nadir is mapped to the sun satellite track which forms a grid edge, this bin is the closest to the right (east) of that. All arrays use 0-base indicies.

<b>BIN_SIZE_IN_KM</b>	Bin width/length at nadir. This is a defined parameter size, independent of pixel size.
-----------------------	---

Table 4 lists the seven fields in the SENSOR\_VIEWS\_BANDS group. This group defines the specific viewing angles (specified at ground), band center wavelengths and bandpasses (Full width, half maximum, FWHM), and the bandpass integrated, annual average, solar irradiance ( $F_0$ ) used to calculate radiometric properties.

Table 4 SENSOR\_VIEWS\_BANDS group

Field	Dimension	Dimension	Unit	Description
VIEW_ANGLES	NUMBER_OF_VIEWS	-	degrees	Along-track view zenith angles for sensor, at sensor*
INTENSITY_WAVELENGTHS	NUMBER_OF_VIEWS	INTENSITY_BANDS_PER_VIEW	nm	Intensity field center wavelengths at each view
INTENSITY_BANDPASSES	NUMBER_OF_VIEWS	INTENSITY_BANDS_PER_VIEW	nm	Intensity field bandpasses at each view, defined as Full Width Half Maximum (FWHM). More details are found in the SPECTRAL_RESPONSE_FUNCTION attribute.
POLARIZATION_WAVELENGTHS	NUMBER_OF_VIEWS	POLARIZATION_BANDS_PER_VIEW	nm	Polarization field center wavelengths at each view
POLARIZATION_BANDPASSES	NUMBER_OF_VIEWS	POLARIZATION_BANDS_PER_VIEW	nm	Polarization field bandpasses at each view
INTENSITY_F0 <sup>#</sup>	NUMBER_OF_VIEWS	INTENSITY_BANDS_PER_VIEW	W m <sup>-2</sup> μm <sup>-1</sup>	Spectral response function convolved mean solar flux at each intensity band and view
POLARIZATION_F0 <sup>#</sup>	NUMBER_OF_VIEWS	POLARIZATION_BANDS_PER_VIEW	W m <sup>-2</sup> μm <sup>-1</sup>	Spectral response function convolved mean solar flux at each polarization band and view

\* VIEW\_ANGLES is defined at the sensor, as it provides a swath independent value at TOA. Definition of view zenith and azimuth angles at the ground, which depend upon bin location and VIEW\_ANGLE, are contained in the SENSOR\_ZENITH and SENSOR\_AZIMUTH fields described below.

<sup>#</sup>Spectral function weighted F0 values may require specification individually for different views, as the spectral response functions for those views may vary. If this is not the case for all instruments, these fields will revert to attributes.

Table 5 contains the characteristics of two fields within the BIN\_ATTRIBUTES group. This group defines the time at which the spacecraft subsatellite point passes over the across track line, and the offsets from that time for all view angles.

Table 5 BIN\_ATTRIBUTES group

Field	Dimension	Dimension	Dimension	Unit	Description
NADIR_VIEW_TIME	BINS_ALONG_TRACK	-	-	Seconds	Time nadir view was observed
VIEW_TIME_OFFSETS	BINS_ALONG_TRACK	BINS_ACROSS_TRACK	NUMBER_OF_VIEWS	Seconds	Offset of view angle time to nadir view time

Table 6 are the fields within the GEOLOCATION\_DATA group, containing bin coordinates, altitude (to which the data have been aggregated) and the solar and sensor geometries. Most conventions are described in Patt and Gregg, (1994). The scattering angle, which is the angle from the solar illumination vector at the bin location to the vector in the direction of the sensor view, is also provided. While SCATTERING\_ANGLE is redundant with other geometry angles,

this parameter is included in the L1C file format definition for consistency and ease of use. It is defined:

$$\begin{aligned}\cos \alpha &= uu_s + (1 - u^2)^{1/2}(1 - u_s^2)^{1/2} \cos(\phi + 180^\circ - \phi_s) \\ u &= \cos(\theta + 180^\circ) \\ u_s &= \cos \theta_s\end{aligned}\tag{1}$$

which uses the convention of equation 3.17 in Hansen and Travis, 1974 but accounts for the definition of geometry that we use (hence the  $180^\circ$  shift for sensor zenith and azimuth angles). An earlier work defining the scattering angle is Hovenier, 1969. In equation (1),  $\alpha$  is the scattering angle,  $\theta$  and  $\theta_s$  are the sensor and solar zenith angles, respectively, and  $\phi$  and  $\phi_s$  are the sensor and solar azimuth angles, respectively (SENSOR\_AZIMUTH, SOLAR\_AZIMUTH). Note that  $180^\circ$  must be added to SENSOR\_ZENITH and SENSOR\_AZIMUTH to align geometry conventions of this document with that of Hansen and Travis, 1974, which considers zenith associated with an upward vector to have a negative sign, and because the associated azimuth angle is rotated  $180^\circ$ . In this convention, scattering angles of  $0^\circ$  and  $180^\circ$  are therefore the forward and backscattered directions, respectively. Figure 4 is a schematic of the geometry conventions.

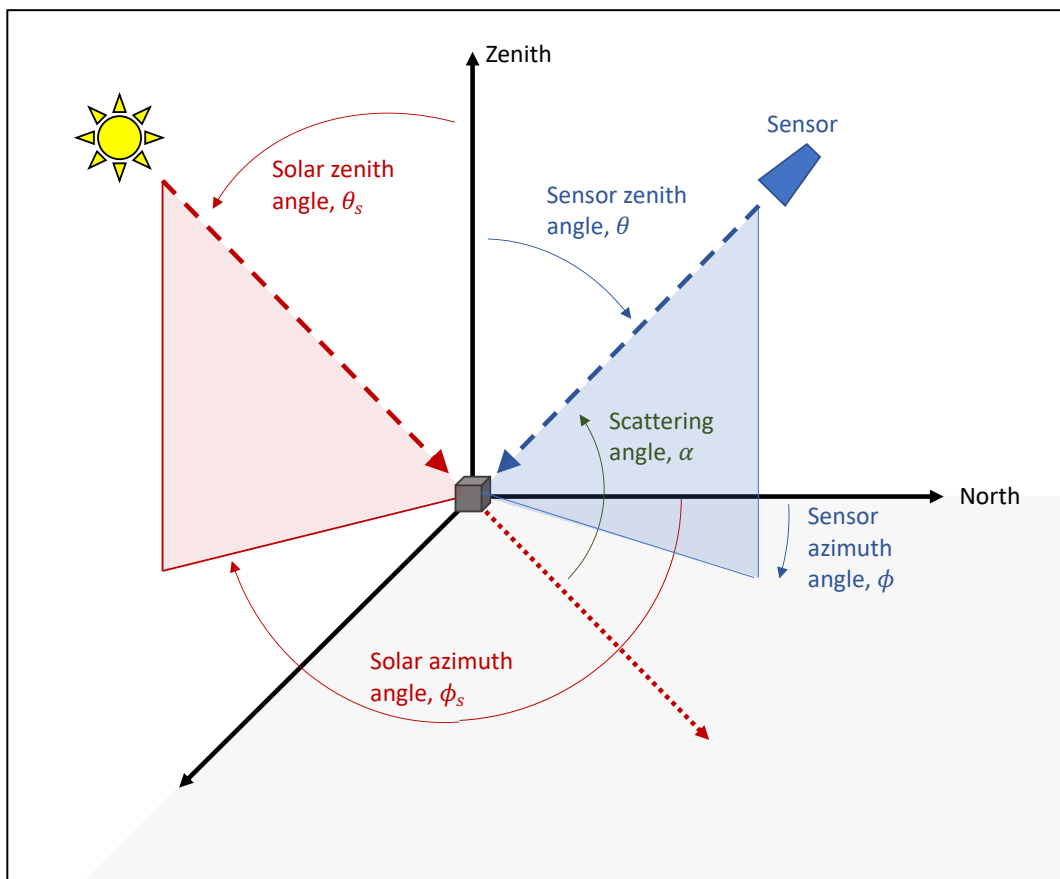


Figure 4 Solar and sensor geometry schematic. Long dashed lines are the solar illumination (red) and sensor view (blue) vectors. The red dotted line is the solar illumination vector continuing past the scattering object (cube). The scattering angle (green) is the angle from that vector to the sensor zenith vector.

**Table 6 GEOLOCATION\_DATA group.**

Field	Dimension	Dimension	Dimension	Unit	Description
LATITUDE	BINS_ALONG_TRACK	BINS_ACROSS_TRACK	-	Degrees North	Latitude of bin location
LONGITUDE	BINS_ALONG_TRACK	BINS_ACROSS_TRACK	-	Degrees East	Longitude of bin location
ALTITUDE	BINS_ALONG_TRACK	BINS_ACROSS_TRACK	-	Meters	(aggregation) altitude of bin location
ALTITUDE_VARIABILITY	BINS_ALONG_TRACK	BINS_ACROSS_TRACK	-	Meters	RMS Variability of terrain altitude within bin
SENSOR_AZIMUTH	BINS_ALONG_TRACK	BINS_ACROSS_TRACK	NUMBER_OF_VIEWS	Degrees	Azimuth angle from the bin location to the sensor, defined clockwise from north. Range: 0° to 360°*
SENSOR_ZENITH	BINS_ALONG_TRACK	BINS_ACROSS_TRACK	NUMBER_OF_VIEWS	Degrees from North	Zenith angle from the bin location to the sensor, defined with respect to the zenith pointing vector. Range: 0° to 90°*
SOLAR_AZIMUTH	BINS_ALONG_TRACK	BINS_ACROSS_TRACK	NUMBER_OF_VIEWS	Degrees from North	Azimuth angle from the bin location to the sun, defined clockwise from north. Range: 0° to 360°*
SOLAR_ZENITH	BINS_ALONG_TRACK	BINS_ACROSS_TRACK	NUMBER_OF_VIEWS	Degrees	Zenith angle from the bin location to the sun, defined with respect to the zenith pointing vector. Range: 0° to 90°*
SCATTERING_ANGLE	BINS_ALONG_TRACK	BINS_ACROSS_TRACK	NUMBER_OF_VIEWS	Degrees	Angle from the sun illumination vector to the vector in the direction of the sensor.

\* we follow the geometry conventions of the PACE SDPS, as described in Patt and Gregg, 1994

**Table 7 OBSERVATION\_DATA group**

Field	Dimension	Dimension	Dimension	Dimension	Unit	Description
OBS_PER_VIEW	BINS_ALONG_TRACK	BINS_ACROSS_TRACK	NUMBER_OF_VIEWS	-	Unitless	Obs. contributing to bin from each view
QC_BITWISE	BINS_ALONG_TRACK	BINS_ACROSS_TRACK	NUMBER_OF_VIEWS	INTENSITY_BANDS_PER_VIEW	Unitless	Bitwise quality indicator
QC	BINS_ALONG_TRACK	BINS_ACROSS_TRACK	NUMBER_OF_VIEWS	INTENSITY_BANDS_PER_VIEW	Unitless	Quality indicator
I	BINS_ALONG_TRACK	BINS_ACROSS_TRACK	NUMBER_OF_VIEWS	INTENSITY_BANDS_PER_VIEW	W m <sup>-2</sup> sr <sup>-1</sup> μm <sup>-1</sup>	I Stokes vector component
I_NOISE	BINS_ALONG_TRACK	BINS_ACROSS_TRACK	NUMBER_OF_VIEWS	INTENSITY_BANDS_PER_VIEW	W m <sup>-2</sup> sr <sup>-1</sup> μm <sup>-1</sup>	Random noise of I in bin
QC_POLSAMPLE_BITWISE	BINS_ALONG_TRACK	BINS_ACROSS_TRACK	NUMBER_OF_VIEWS	POLARIZATION_BANDS_PER_VIEW	Unitless	Bitwise quality indicator
QC_POLSAMPLE	BINS_ALONG_TRACK	BINS_ACROSS_TRACK	NUMBER_OF_VIEWS	POLARIZATION_BANDS_PER_VIEW	Unitless	Quality indicator
I_POLSAMPLE	BINS_ALONG_TRACK	BINS_ACROSS_TRACK	NUMBER_OF_VIEWS	POLARIZATION_BANDS_PER_VIEW	W m <sup>-2</sup> sr <sup>-1</sup> μm <sup>-1</sup>	I Stokes vector component at polarimeter

						spectral sampling
I_POLSAMPLE NOISE	BINS_ALONG_T RACK	BINS_ACROSS_T RACK	NUMBER_OF_VIEWS	POLARIZATION_BANDS_P ER_VIEW	$W m^{-2} sr^{-1} \mu m^{-1}$	Random noise of I_POLSAMPLE in bin
Q	BINS_ALONG_T RACK	BINS_ACROSS_T RACK	NUMBER_OF_VIEWS	POLARIZATION_BANDS_P ER_VIEW	$W m^{-2} sr^{-1} \mu m^{-1}$	Q Stokes vector component
Q_NOISE	BINS_ALONG_T RACK	BINS_ACROSS_T RACK	NUMBER_OF_VIEWS	POLARIZATION_BANDS_P ER_VIEW	$W m^{-2} sr^{-1} \mu m^{-1}$	Random noise of Q in bin
U	BINS_ALONG_T RACK	BINS_ACROSS_T RACK	NUMBER_OF_VIEWS	POLARIZATION_BANDS_P ER_VIEW	$W m^{-2} sr^{-1} \mu m^{-1}$	U Stokes vector component
U_NOISE	BINS_ALONG_T RACK	BINS_ACROSS_T RACK	NUMBER_OF_VIEWS	POLARIZATION_BANDS_P ER_VIEW	$W m^{-2} sr^{-1} \mu m^{-1}$	Random noise of U in bin
Q_OVER_I	BINS_ALONG_T RACK	BINS_ACROSS_T RACK	NUMBER_OF_VIEWS	POLARIZATION_BANDS_P ER_VIEW	Unitless	Q over I (little q) Stokes vector component
Q_OVER_I_NOISE	BINS_ALONG_T RACK	BINS_ACROSS_T RACK	NUMBER_OF_VIEWS	POLARIZATION_BANDS_P ER_VIEW	Unitless	Random noise of Q_OVER_I in bin
U_OVER_I	BINS_ALONG_T RACK	BINS_ACROSS_T RACK	NUMBER_OF_VIEWS	POLARIZATION_BANDS_P ER_VIEW	Unitless	U over I (little u) Stokes vector component
U_OVER_I_NOISE	BINS_ALONG_T RACK	BINS_ACROSS_T RACK	NUMBER_OF_VIEWS	POLARIZATION_BANDS_P ER_VIEW	Unitless	Random noise of U_OVER_I in bin
DOLP	BINS_ALONG_T RACK	BINS_ACROSS_T RACK	NUMBER_OF_VIEWS	POLARIZATION_BANDS_P ER_VIEW	Unitless	Degree of linear polarization
DOLP_NOISE	BINS_ALONG_T RACK	BINS_ACROSS_T RACK	NUMBER_OF_VIEWS	POLARIZATION_BANDS_P ER_VIEW	Unitless	Random noise of DOLP in bin
AOLP	BINS_ALONG_T RACK	BINS_ACROSS_T RACK	NUMBER_OF_VIEWS	POLARIZATION_BANDS_P ER_VIEW	degrees	Angle of linear polarization
AOLP_NOISE	BINS_ALONG_T RACK	BINS_ACROSS_T RACK	NUMBER_OF_VIEWS	POLARIZATION_BANDS_P ER_VIEW	degrees	Random noise of AOLP in bin

Table 7 contains the OBSERVATION\_DATA group. As the name suggests, this group contains the core data fields, which also have the largest dimensionality (4D). The L1C file is to contain data from instruments with sensitivity to linear polarization, which we represent with the Stokes' vector:

$$\mathbf{I} = \begin{bmatrix} I = \langle E_l E_l^* + E_r E_r^* \rangle \\ Q = \langle E_l E_l^* - E_r E_r^* \rangle \\ U = \langle E_l E_r^* + E_r E_l^* \rangle \\ V = i \langle E_l E_r^* - E_r E_l^* \rangle \end{bmatrix} \quad (1)$$

Here, the brackets indicate phase average and the \* the complex conjugate of an electric field represented by a pair of mutually perpendicular oscillating components,  $E_l$  and  $E_r$  :

$$\begin{aligned} E_l &= a_l e^{i(\omega t - kz - \epsilon_l)} \\ E_r &= a_r e^{i(\omega t - kz - \epsilon_r)} \end{aligned} \quad (2)$$

These components are each associated with unit vectors  $\mathbf{r}$  and  $\mathbf{l}$  (whose cross product is the propagation direction,  $z$  is distance in this direction), and where  $k$  is the wave number,  $t$  is time,  $\omega$  is frequency,  $a_l$  and  $a_r$  are wave amplitudes, and  $\epsilon_l$  and  $\epsilon_r$  are phases (Hansen et al., 1974).

In a practical sense, the  $I$  component of the Stokes vector represents the total intensity (a term we use loosely without defining units), while  $Q$  and  $U$  contain information about the direction and magnitude of linear polarization. Circular polarization is expressed with  $V$ , which is henceforth omitted since none of the PACE instruments are sensitive to this parameter.

Equations (1) and (2) show that  $Q$  and  $U$  are defined with respect to a reference plane, which for the L1C file we define to be in the spacecraft meridional plane (containing unit vectors in the nadir and spacecraft heading directions). Hovenier and van der Mee (1983) describe the calculations required to convert  $Q$  and  $U$  to other reference planes, such as the solar scattering plane.

A commonly used polarimetric quantity is the Degree of Linear Polarization (DoLP):

$$DoLP = \frac{\sqrt{Q^2 + U^2}}{I} \quad (3)$$

which has the benefit of condensing  $Q$  and  $U$  into a single, reference plane insensitive, parameter. While this does represent a loss of information, in many observation systems (including the PACE MAPS) some systematic uncertainties cancel when represented by DoLP, leading to low relative uncertainty. Assessment of the polarization angle can be represented by the Angle of Linear Polarization (AoLP):

$$AoLP = \frac{1}{2} \tan^{-1} \frac{U}{Q} \quad (4)$$

where we adopt the common convention (Hansen and Travis, 1974) to select the value in the interval  $0 \leq AoLP \leq \pi$  for which  $\cos(2AoLP)$  has the same sign as  $Q$ .

An alternative  $Q$  and  $U$  formulation, which takes advantage of normalization with respect to  $I$ , but preserves the sign and direction in  $Q$  and  $U$ , is:

$$q = \frac{Q}{I}; u = \frac{U}{I} \quad (5)$$

Depending on the application, L1C to L2 algorithms may have a preference for one or another representation of the polarimetric state. Furthermore, different instruments may vary in the inherent polarimetric measurement that is made. In our case, HARP2 data are produced as  $Q$  and  $U$ , while for SPEXone it is  $q$  and  $u$ . Furthermore, the spectral sampling (and resolution) for SPEXone varies for  $I$ ,  $q$  and  $u$  (see Table 1;  $I$  has higher spectral resolution than  $q$  and  $u$ ).

Conversion of SPEXone  $q$  and  $u$  to  $Q$  and  $U$  or  $DoLP$ , therefore, requires using  $I$  that has been spectrally sampled like  $q$  and  $u$ , which we call  $I\_POLSAMPLE$ .

To balance the competing desire to contain polarimetric data as measured, provide for an accurate conversion to the variety of polarimetric forms that might be used in an algorithm and do so in as compact a manner possible, we intend to fill fields in Table 7 differently for each instrument, as follows:

**OCI:** I

**HARP2:** I; Q; U

**SPEXone:** I;  $I\_POLSAMPLE$ ;  $Q\_OVER\_I$ ;  $U\_OVER\_I$

**Redundant but convenient:** DoLP, AoLP

In this way, HARP2 data can be easily converted to  $q$  and  $u$  using equation (5). SPEXone data can be converted to  $Q$  and  $U$  by inverting equation (5) and using  $I\_POLSAMPLE$  ( $I$  resampled on the  $q$  and  $u$  spectral sensitivity).

Measurement uncertainty can be quite variable for polarization, and also different than for  $I$ . Algorithms that utilize polarimetric data need (unique) measurement uncertainty estimates to properly weight the different types of data that are used. Therefore, the  $\_NOISE$  fields are used to represent the component of measurement uncertainty due to random errors. There would be combined (added in quadrature, presumably) with estimates of systematic uncertainty from the  $SYSTEMATIC\_UNCERTAINTY\_MODEL$  attribute (see Knobelspiesse et al., 2019 for examples of uncertainty models for MAPs).

$I$ ,  $Q$ , and  $U$  have units of radiance, ( $W\ sr^{-1}\ m^{-2}$  per  $\mu m$ ). Conversion to (unitless) reflectance is performed by calculating

$$R_{[I,Q,U]} = \frac{[I, Q, U]\pi r^2}{F_0 \cos \theta_s} \quad (6)$$

Where  $r$  is the sun earth distance relative to the distance at which  $F_0$  is defined (in  $SUN\_EARTH\_DISTANCE$  global attribute),  $F_0$  is the mean solar flux in  $W/m^2$  ( $INTENSITY\_F0$  or  $POLARIZATION\_F0$ ), and  $\theta_s$  is the solar zenith angle ( $SOLAR\_ZENITH$ ).

Quality indicators will be used to indicate the level of data quality for a particular bin. These include a bitwise quality indicator ( $QC\_BITWISE$ ,  $QC\_POLSAMPLE\_BITWISE$ ) which have bits indicating specific quality issues, such as swath edge, geolocation uncertainty, and otherwise. Those bitwise indicators can be combined to a single quality level based upon instrument team specific preferences. For example, HARP2 data could have ( $QC$  or  $QC\_POLSAMPLE$ ) in the scale of 0-3, where 0 indicates optimal conditions, and larger numbers indicate less optimal conditions. Regardless of instrument or scheme, all will use 0 as an

indicator of highest quality, so that changes to the quality level scheme are backwards compatible for the highest quality level.

## 7 EXTERNAL DATA AND SOFTWARE

### 7.1 Re-aggregation tool

A software tool will be provided that can be used to re-aggregate the data to a different altitude, and provide a modified L1C product representative of that altitude. The default aggregation altitude in L1C files is the surface, as specified by the terrain height on land and the ellipsoid over the ocean. This tool will take L1B files as input.

### 7.2 Downsampling tool

L1C files may have spatial grids that differ for each instrument. While these grids have been chosen to be multiples of each other to ease intercomparison, a tool will be provided that can downsample a given file's data to a lower spatial resolution, while preserving the correct geometry and other relevant fields. For example, a user might choose to utilize SPEXone and OCI data together. The former has a spatial grid of 2.6km<sup>2</sup>, the latter 5.2km<sup>2</sup>. Thus, the downsampling tool would take as input a SPEXone file gridded at 2.6km<sup>2</sup> and generate one at 5.2km<sup>2</sup>.

### 7.3 Ancillary and OCI derived data on the L1C grid

Some L1C to L2 algorithms will require either derived or ancillary data on the L1C grid. Those data will be kept in a separate file (L1C-ancillary) which has the same GEOLOCATION\_DATA group as the L1C files, but a different OBSERVATION\_DATA group containing the following fields:

1. OCI derived cloud fraction
2. OCI derived cloud phase
3. OCI derived cloud top height
4. [SOME OTHER ALGORITHM] derived cloud top height
5. [SOME ALGORITHM] derived aerosol layer height
6. OCI derived Cloud Effective Radius
7. Ancillary data from MERRA: O3 profile, NO2 profile, temperature profile, pressure profile, relative (or specific) humidity profile.

## 8 REFERENCES

Böhm, C., Sourdeval, O., Mülmenstädt, J., Quaas, J., and Crewell, S., 2019. Cloud base height retrieval from multi-angle satellite data, *Atmos. Meas. Tech.*, 12, 1841–1860, <https://doi.org/10.5194/amt-12-1841-2019>.

Diner, D.J., Beckert, J.C., Reilly, T.H., Bruegge, C.J., Conel, J.E., Kahn, R.A., Martonchik, J.V., Ackerman, T.P., Davies, R., Gerstl, S.A. and Gordon, H.R., 1998. Multi-angle Imaging

SpectroRadiometer (MISR) instrument description and experiment overview. *IEEE Transactions on Geoscience and Remote Sensing*, 36(4), pp.1072-1087.

Engels, J. and Grafarend, E. 1995. The oblique Mercator projection of the ellipsoid of revolution IE a 2, b, *Journal of Geodesy*, 70(1-2), 38--50.

Frouin, R. J., B. A. Franz, A. Ibrahim, K. Knobelspiesse, Z. Ahmad, B. Cairns, J. Chowdhary, H. M. Dierssen, J. Tan, O. Dubovik, X. Huang, A. B. Davis, O. Kalashnikova, D. R. Thompson, L. A. Remer, E. Boss, O. Coddington, P.-Y. Deschamps, B.-C. Gao, L. Gross, O. Hasekamp, A. Omar, B. Pelletier, D. Ramon, F. Steinmetz, and P.-W. Zhai. 2019. Atmospheric Correction of Satellite Ocean-Color Imagery During the PACE Era. *Frontiers in Earth Science*, 7: [10.3389/feart.2019.00145]

Gelaro, R., McCarty, W., Suárez, M. J., Todling, R., Molod, A., Takacs, L., Randles, C. A., Darmenov, A., Bosilovich, M. G., Reichle, R., and others 2017. The modern-era retrospective analysis for research and applications, version 2 (MERRA-2), *Journal of Climate*, 30(14), 5419--5454.

Hansen, J.E. and Travis, L.D., 1974. Light scattering in planetary atmospheres. *Space science reviews*, 16(4), pp.527-610.

Hasekamp, O.P., Fu, G., Rusli, S.P., Wu, L., Di Noia, A., aan de Brugh, J., Landgraf, J., Smit, J.M., Rietjens, J. and van Amerongen, A., 2019. Aerosol measurements by SPEXone on the NASA PACE mission: expected retrieval capabilities. *Journal of Quantitative Spectroscopy and Radiative Transfer*, 227, pp.170-184.

Hovenier, J. W.: Symmetry Relationships for Scattering of Polarized Light in a Slab of Randomly Oriented Particles, *J. Atmos. Sci.*, 26(3), 488--499, 1969.

Hovenier, J.W. and Van der Mee, C.V.M., 1983. Fundamental relationships relevant to the transfer of polarized light in a scattering atmosphere. *Astronomy and Astrophysics*, 128, pp.1-16.

Knobelspiesse, K., Q. Tan, C. Bruegge, B. Cairns, J. Chowdhary, B. van Diedenhoven, D. Diner, R. Ferrare, G. van Harten, V. Jovanovic, M. Ottaviani, J. Redemann, F. Seidel, and K. Sinclair. 2019. Intercomparison of airborne multi-angle polarimeter observations from the Polarimeter Definition Experiment. *Applied Optics*, 58 (3): 650 [10.1364/ao.58.000650]

Lang, R., Poli, G., Fougnie, B., Lacan, A., Marbach, T., Riedi, J., Schlüssel, P., Couto, A. and Munro, R., 2019. The 3MI Level-1C geoprojected product–definition and processing description. *Journal of Quantitative Spectroscopy and Radiative Transfer*, 225, pp.91-109.

Martins, J.V., Fernandez-Borda, R., McBride, B., Remer, L. and Barbosa, H.M., 2018, July. The Harp Hype Ran Gular Imaging Polarimeter and the Need for Small Satellite Payloads with High Science Payoff for Earth Science Remote Sensing. In *IGARSS 2018-2018 IEEE International Geoscience and Remote Sensing Symposium* (pp. 6304-6307). IEEE.

- Moroney, C., Davies, R. and Muller, J.P., 2002. Operational retrieval of cloud-top heights using MISR data. *IEEE Transactions on Geoscience and Remote Sensing*, 40(7), pp.1532-1540.
- Nelson, D., Garay, M., Kahn, R. and Dunst, B., 2013. Stereoscopic height and wind retrievals for aerosol plumes with the MISR INteractive eXplorer (MINX). *Remote Sensing*, 5(9), pp.4593-4628.
- Patt, F. S. and Gregg, W. W., 1994. Exact closed-form geolocation algorithm for Earth survey sensors, *Int. J. Remote Sens.*, 15(18), 3719-3734 , <https://doi.org/10.1080/01431169408954354>, 1994.
- Remer, L. A., K. Knobelspiesse, P.-W. Zhai, F. Xu, O. V. Kalashnikova, J. Chowdhary, O. Hasekamp, O. Dubovik, L. Wu, Z. Ahmad, E. Boss, B. Cairns, O. Coddington, A. B. Davis, H. M. Dierssen, D. J. Diner, B. Franz, R. Frouin, B.-C. Gao, A. Ibrahim, R. C. Levy, J. V. Martins, A. H. Omar, and O. Torres. 2019. Retrieving Aerosol Characteristics From the PACE Mission, Part 2: Multi-Angle and Polarimetry. *Frontiers in Environmental Science*, 7: [10.3389/fenvs.2019.00094]
- Sayer, A.M. and Knobelspiesse, K.D., 2019. How should we aggregate data? Methods accounting for the numerical distributions, with an assessment of aerosol optical depth. *Atmospheric Chemistry and Physics*, 19(23), pp.15023-15048.
- Sinclair, K., B. van Diedenhoven, B. Cairns, J. Yorks, A. Wasilewski, and M. McGill, 2017: Remote sensing of multiple cloud layer heights using multi-angular measurements. *Atmos. Meas. Tech.*, 10, 2361-2375, doi:10.5194/amt-10-2361-2017.
- Snyder, J. P. 1978: The space oblique Mercator projection, *Photogramm. Eng. Remote Sensing*, 44, 585-596, 140.
- Snyder, J.P., 1987. *Map projections--A working manual* (Vol. 1395). US Government Printing Office.
- Werdell, P. J., M. J. Behrenfeld, P. S. Bontempi, E. Boss, B. Cairns, G. T. Davis, B. A. Franz, U. B. Gliese, E. T. Gorman, O. Hasekamp, K. D. Knobelspiesse, A. Mannino, J. V. Martins, C. R. McClain, G. Meister, and L. A. Remer. 2019. The Plankton, Aerosol, Cloud, ocean Ecosystem (PACE) mission: Status, science, advances. *Bulletin of the American Meteorological Society*, 100 (9): 1775–1794 [10.1175/bams-d-18-0056.1]

## 9 APPENDIX A: ACRONYMS

AoLP	Angle of Linear Polarization
CDL	Common Data Label
DEM	Digital Elevation Model
DNH	Do-No-Harm
DoLP	Degree of Linear Polarization

FWHM	Full width, half maximum
HARP2	Hyper-Angular Rainbow Polarimeter-2
L1C	Level 1c
L2	Level 2
MAP	Multi-angle polarimeter
MISR	Multi-angle Imaging SpectroRadiometer
MODIS	Moderate Resolution Imaging Spectroradiometer
OBPG	Ocean Biology Processing Group
OB-DAAC	Ocean Biology Distributed Active Archive Center
OCI	Ocean Color Instrument
PACE	Plankton, Aerosol, Cloud, ocean Ecosystem
SOCEA	Spacecraft Oblique Cylindrical Equal Area
SPEXone	Spectro-Polarimeter for Planetary Exploration-one
TBD	To be determined
TOA	Top of Atmosphere

## 10 APPENDIX B: SAMPLE CDL FOR HARP2

```

netcdf PACE_HARP2.20220301T123621.L1C.5.2km {
dimensions:
    number_of_views = 90 ;
    intensity_bands_per_view = 1 ;
    polarization_bands_per_view = 1 ;
    bins_along_track = 4000 ;
    bins_across_track = 600 ;

// global attributes:
    :title = "PACE HARP2 Level-1C Data" ;
    :instrument = "HARP2" ;
    :processing_version = "V1.0" ;
    :Conventions = "CF-1.6" ;
    :institution = "NASA Goddard Space Flight Center, Ocean Biology Processing Group" ;
    :license = "http://science.nasa.gov/earth-science/earth-science-data/data-information-policy/" ;
    :naming_authority = "gov.nasa.gsfc.sci.oceancolor" ;
    :keywords_vocabulary = "NASA Global Change Master Directory (GCMD) Science Keywords" ;
    :stdname_vocabulary = "NetCDF Climate and Forecast (CF) Metadata Convention" ;
    :creator_name = "NASA/GSFC" ;
    :creator_email = "data@oceancolor.gsfc.nasa.gov" ;
    :creator_url = "http://oceancolor.gsfc.nasa.gov" ;
    :project = "PACE Project" ;
    :publisher_name = "NASA/GSFC" ;
    :publisher_email = "data@oceancolor.gsfc.nasa.gov" ;
    :publisher_url = "http://oceancolor.gsfc.nasa.gov" ;
    :processing_level = "L1C" ;
    :cdm_data_type = "swath" ;
    :orbit_number = 12345 ;
    :history = "" ;
    :CDL_version_date = "2020-02-28" ;
    :product_name = "PACE_HARP2.20220301T123621.L1C.5.2km.nc" ;
    :startDirection = "Descending" ;
    :endDirection = "Ascending" ;
    :time_coverage_start = "2022-03-01T12:36:21Z" ;
    :time_coverage_end = "2022-03-01T13:26:57Z" ;
    :date_created = "2020-03-05T15:12:41Z" ;
    :sun_earth_distance = 0.990849042172323 ;
    :terrain_data_source = "" ;
    :spectral_response_function = "" ;
    :systematic_uncertainty_model = "" ;
    :nadir_bin = 12345 ;
    :bin_size_at_nadir = 5.2km2

group: sensor_views_bands {
variables:
    float view_angles(number_of_views) ;
        view_angles:long_name = "Along-track view angles for sensor" ;
        view_angles:units = "degrees" ;
        view_angles:FillValue = -999.f ;
        view_angles:valid_min = -89. ;
        view_angles:valid_max = 89. ;
    float intensity_wavelengths(number_of_views, intensity_bands_per_view) ;
        intensity_wavelengths:long_name = "Intensity field center wavelengths at each view" ;
        intensity_wavelengths:units = "nm" ;
        intensity_wavelengths:FillValue = -999.f ;
        intensity_wavelengths:valid_min = 320. ;
        intensity_wavelengths:valid_max = 2260. ;
    float intensity_bandpasses(number_of_views, intensity_bands_per_view) ;
        intensity_bandpasses:long_name = "Intensity field bandpasses at each view" ;

```

```

        intensity_bandpasses:units = "nm" ;
        intensity_bandpasses:_FillValue = -999.f ;
        intensity_bandpasses:valid_min = 2.5 ;
        intensity_bandpasses:valid_max = 100. ;
float polarization_wavelengths(number_of_views, polarization_bands_per_view) ;
    polarization_wavelengths:long_name = "Polarization field wavelengths at each view" ;
    polarization_wavelengths:units = "nm" ;
    polarization_wavelengths:_FillValue = -999.f ;
    polarization_wavelengths:valid_min = 320. ;
    polarization_wavelengths:valid_max = 2260. ;
float polarization_bandpasses(number_of_views, polarization_bands_per_view) ;
    polarization_bandpasses:long_name = "Polarization field bandpasses at each view" ;
    polarization_bandpasses:units = "nm" ;
    polarization_bandpasses:_FillValue = -999.f ;
    polarization_bandpasses:valid_min = 2.5 ;
    polarization_bandpasses:valid_max = 100. ;
float intensity_F0(number_of_views, intensity_bands_per_view) ;
    intensity_F0:long_name = "Intensity band solar irradiance" ;
    intensity_F0:units = "W m^-2 μm^-1" ;
    intensity_F0:_FillValue = -999.f ;
    intensity_F0:valid_min = 0. ;
    intensity_F0:valid_max = 900. ;
float polarization_F0(number_of_views, polarization_bands_per_view) ;
    polarization_F0:long_name = "Polarization band solar irradiance" ;
    polarization_F0:units = "W m^-2 μm^-1" ;
    polarization_F0:_FillValue = -999.f ;
    polarization_F0:valid_min = 0. ;
    polarization_F0:valid_max = 900. ;
} // group sensor_views_bands

group: bin_attributes {
    variables:
        double nadir_view_time(bins_along_track) ;
            nadir_view_time:long_name = "Time bin was viewed at nadir view" ;
            nadir_view_time:units = "seconds" ;
            nadir_view_time:_FillValue = -999. ;
            nadir_view_time:valid_min = 0. ;
            nadir_view_time:valid_max = 86400.999 ;
        double view_time_offsets(bins_along_track, bins_across_track, number_of_views) ;
            view_time_offsets:long_name = "Time offsets of views from nadir view" ;
            view_time_offsets:units = "seconds" ;
            view_time_offsets:_FillValue = -999. ;
            view_time_offsets:valid_min = -200. ;
            view_time_offsets:valid_max = 200. ;
} // group bin_attributes

group: geolocation_data {
    variables:
        float latitude(bins_along_track, bins_across_track) ;
            latitude:long_name = "Latitudes of bin locations" ;
            latitude:units = "degrees_north" ;
            latitude:_FillValue = -999.f ;
            latitude:valid_min = -90.f ;
            latitude:valid_max = 90.f ;
        float longitude(bins_along_track, bins_across_track) ;
            longitude:long_name = "Longitudes of bin locations" ;
            longitude:units = "degrees_east" ;
            longitude:_FillValue = -999.f ;
            longitude:valid_min = -180.f ;
            longitude:valid_max = 180.f ;
        short altitude(bins_along_track, bins_across_track) ;

```

```
    altitude:long_name = "Altitude at bin locations" ;
    altitude:units = "meters" ;
    altitude:_FillValue = -32768s ;
    altitude:valid_min = -1000s ;
    altitude:valid_max = 10000s ;
    altitude:scale_factor = 1.f ;
    altitude:add_offset = 0.f ;
short altitude_variability(bins_along_track, bins_across_track) ;
    altitude_variability:long_name = "RMS variability of altitude at bin locations" ;
    altitude_variability:units = "meters" ;
    altitude_variability:_FillValue = -32768s ;
    altitude_variability:valid_min = 0s ;
    altitude_variability:valid_max = 1000s ;
    altitude_variability:scale_factor = 1.f ;
    altitude_variability:add_offset = 0.f ;
short sensor_azimuth(bins_along_track, bins_across_track, number_of_views) ;
    sensor_azimuth:long_name = "Sensor azimuth angles at bin locations" ;
    sensor_azimuth:units = "degrees from north" ;
    sensor_azimuth:_FillValue = -32768s ;
    sensor_azimuth:valid_min = -18000s ;
    sensor_azimuth:valid_max = 18000s ;
    sensor_azimuth:scale_factor = 0.01f ;
    sensor_azimuth:add_offset = 0.f ;
short sensor_zenith(bins_along_track, bins_across_track, number_of_views) ;
    sensor_zenith:long_name = "Sensor zenith angles at bin locations" ;
    sensor_zenith:units = "degrees" ;
    sensor_zenith:_FillValue = -32768s ;
    sensor_zenith:valid_min = 0s ;
    sensor_zenith:valid_max = 18000s ;
    sensor_zenith:scale_factor = 0.01f ;
    sensor_zenith:add_offset = 0.f ;
short solar_azimuth(bins_along_track, bins_across_track, number_of_views) ;
    solar_azimuth:long_name = "Solar azimuth angle at bin locations" ;
    solar_azimuth:units = "degrees from north" ;
    solar_azimuth:_FillValue = -32768s ;
    solar_azimuth:valid_min = -18000s ;
    solar_azimuth:valid_max = 18000s ;
    solar_azimuth:scale_factor = 0.01f ;
    solar_azimuth:add_offset = 0.f ;
short solar_zenith(bins_along_track, bins_across_track, number_of_views) ;
    solar_zenith:long_name = "Solar zenith angle at bin locations" ;
    solar_zenith:units = "degrees" ;
    solar_zenith:_FillValue = -32768s ;
    solar_zenith:valid_min = 0s ;
    solar_zenith:valid_max = 18000s ;
    solar_zenith:scale_factor = 0.01f ;
    solar_zenith:add_offset = 0.f ;
short scattering_angle(bins_along_track, bins_across_track, number_of_views) ;
    scattering_angle:long_name = "Scattering angle at bin locations" ;
    scattering_angle:units = "degrees" ;
    scattering_angle:_FillValue = -32768s ;
    scattering_angle:valid_min = 0s ;
    scattering_angle:valid_max = 18000s ;
    scattering_angle:scale_factor = 0.01f ;
    scattering_angle:add_offset = 0.f ;

} // group geolocation_data

group: observation_data {
  variables:
    short obs_per_view(bins_along_track, bins_across_track, number_of_views) ;
```

```

    obs_per_view:long_name = "Observations contributing to bin from each view" ;
    obs_per_view:valid_min = 0 ;
    obs_per_view:valid_max = 999 ;
float QC_bitwise(bins_along_track, bins_across_track, number_of_views, intensity_bands_per_view) ;
    QC_bitwise:long_name = "bitwise quality indicator" ;
    QC_bitwise:units = "unitless" ;
    QC_bitwise:FillValue = 0.b;
    QC_bitwise:valid_min = 0.b;
    QC_bitwise:valid_max = 02^16.b;
float QC(bins_along_track, bins_across_track, number_of_views, intensity_bands_per_view) ;
    QC:long_name = "quality indicator" ;
    QC:units = "unitless" ;
    QC:FillValue = 0.i;
    QC:valid_min = 0.i;
    QC:valid_max = 10i;
float I(bins_along_track, bins_across_track, number_of_views, intensity_bands_per_view) ;
    I:long_name = "I Stokes vector component" ;
    I:units = "W m^-2 sr^-1 um^-1" ;
    I:FillValue = -999.f ;
    I:valid_min = 0.f ;
    I:valid_max = 999.f ;
float I_noise(bins_along_track, bins_across_track, number_of_views, intensity_bands_per_view) ;
    I_noise:long_name = "Random noise of I in bin" ;
    I_noise:units = "W m^-2 sr^-1 um^-1" ;
    I_noise:FillValue = -999.f ;
    I_noise:valid_min = 0.f ;
    I_noise:valid_max = 800.f ;
float Q(bins_along_track, bins_across_track, number_of_views, polarization_bands_per_view) ;
    Q:long_name = "Q Stokes vector component" ;
    Q:units = "W m^-2 sr^-1 um^-1" ;
    Q:FillValue = -999.f ;
    Q:valid_min = -800.f ;
    Q:valid_max = 800.f ;
float Q_noise(bins_along_track, bins_across_track, number_of_views, polarization_bands_per_view) ;
    Q_noise:long_name = "Random noise of Q in bin" ;
    Q_noise:units = "W m^-2 sr^-1 um^-1" ;
    Q_noise:FillValue = -999.f ;
    Q_noise:valid_min = 0.f ;
    Q_noise:valid_max = 800.f ;
float U(bins_along_track, bins_across_track, number_of_views, polarization_bands_per_view) ;
    U:long_name = "U Stokes vector component" ;
    U:units = "W m^-2 sr^-1 um^-1" ;
    U:FillValue = -999.f ;
    U:valid_min = -800.f ;
    U:valid_max = 800.f ;
float U_noise(bins_along_track, bins_across_track, number_of_views, polarization_bands_per_view) ;
    U_noise:long_name = "Random noise of U in bin" ;
    U_noise:units = "W m^-2 sr^-1 um^-1" ;
    U_noise:FillValue = -999.f ;
    U_noise:valid_min = 0.f ;
    U_noise:valid_max = 800.f ;
float DOLP(bins_along_track, bins_across_track, number_of_views, polarization_bands_per_view) ;
    DOLP:long_name = "Degree of linear polarization" ;
    DOLP:FillValue = -999.f ;
    DOLP:valid_min = 0.f ;
    DOLP:valid_max = 1.f ;
float DOLP_noise(bins_along_track, bins_across_track, number_of_views, polarization_bands_per_view) ;
    DOLP_noise:long_name = "Random noise of DOLP in bin" ;
    DOLP_noise:FillValue = -999.f ;
    DOLP_noise:valid_min = 0.f ;
    DOLP_noise:valid_max = 1.f ;

```

```
float AOLP(bins_along_track, bins_across_track, number_of_views, polarization_bands_per_view) ;
    AOLP:long_name = "Angle of linear polarization" ;
    AOLP:units = degrees;
    AOLP:_FillValue = -999.f;
    AOLP:valid_min = 0.f;
    AOLP:valid_max = 360.f;
float AOLP_noise(bins_along_track, bins_across_track, number_of_views, polarization_bands_per_view) ;
    AOLP_noise:long_name = "Random noise of AOLP in bin" ;
    AOLP_noise:units = degrees;
    AOLP_noise:_FillValue = -999.f;
    AOLP_noise:valid_min = 0.f;
    AOLP_noise:valid_max = 360.f;

} // group observation_data
}
```

## 11 APPENDIX C: SAMPLE CDL FOR OCI

```

netcdf PACE_OCI.20220301T123621.L1C.5.2km {
dimensions:
    number_of_views = 2 ;
    intensity_bands_per_view = 249 ;
    bins_along_track = 4000 ;
    bins_across_track = 514 ;

// global attributes:
    :title = "PACE OCI Level-1C Data" ;
    :instrument = "OCI" ;
    :processing_version = "V1.0" ;
    :Conventions = "CF-1.6" ;
    :institution = "NASA Goddard Space Flight Center, Ocean Biology Processing Group" ;
    :license = "http://science.nasa.gov/earth-science/earth-science-data/data-information-policy/" ;
    :naming_authority = "gov.nasa.gsfc.sci.oceancolor" ;
    :keywords_vocabulary = "NASA Global Change Master Directory (GCMD) Science Keywords" ;
    :stdname_vocabulary = "NetCDF Climate and Forecast (CF) Metadata Convention" ;
    :creator_name = "NASA/GSFC" ;
    :creator_email = "data@oceancolor.gsfc.nasa.gov" ;
    :creator_url = "http://oceancolor.gsfc.nasa.gov" ;
    :project = "PACE Project" ;
    :publisher_name = "NASA/GSFC" ;
    :publisher_email = "data@oceancolor.gsfc.nasa.gov" ;
    :publisher_url = "http://oceancolor.gsfc.nasa.gov" ;
    :processing_level = "L1C" ;
    :cdm_data_type = "swath" ;
    :orbit_number = 12345 ;
    :history = "" ;
    :CDL_version_date = "2020-02-28" ;
    :product_name = "PACE_OCI.20220301T123621.L1C.5.2km.nc" ;
    :startDirection = "Descending" ;
    :endDirection = "Ascending" ;
    :time_coverage_start = "2022-03-01T12:36:21Z" ;
    :time_coverage_end = "2022-03-01T13:26:57Z" ;
    :date_created = "2020-03-05T15:12:41Z" ;
    :sun_earth_distance = 0.990849042172323 ;
    :terrain_data_source = "" ;
    :spectral_response_function = "" ;
    :systematic_uncertainty_model = "" ;
    :nadir_bin = 12345 ;
    :bin_size_at_nadir = 2.6km2

group: sensor_views_bands {
variables:
    float view_angles(number_of_views) ;
        view_angles:long_name = "Along-track view angles for sensor" ;
        view_angles:units = "degrees" ;
        view_angles:FillValue = -999.f ;
        view_angles:valid_min = -89. ;
        view_angles:valid_max = 89. ;
    float intensity_wavelengths(number_of_views, intensity_bands_per_view) ;
        intensity_wavelengths:long_name = "Intensity field center wavelengths at each view" ;
        intensity_wavelengths:units = "nm" ;
        intensity_wavelengths:FillValue = -999.f ;
        intensity_wavelengths:valid_min = 320. ;
        intensity_wavelengths:valid_max = 2260. ;
    float intensity_bandpasses(number_of_views, intensity_bands_per_view) ;
        intensity_bandpasses:long_name = "Intensity field bandpasses at each view" ;
        intensity_bandpasses:units = "nm" ;

```

```

        intensity_bandpasses:_FillValue = -999.f;
        intensity_bandpasses:valid_min = 2.5;
        intensity_bandpasses:valid_max = 100;
    float intensity_F0(number_of_views, intensity_bands_per_view);
        intensity_F0:long_name = "Intensity band solar irradiance";
        intensity_F0:units = "W m^-2 μm^-1";
        intensity_F0:_FillValue = -999.f;
        intensity_F0:valid_min = 0;
        intensity_F0:valid_max = 900;
} // group sensor_views_bands

group: bin_attributes {
    variables:
        double nadir_view_time(bins_along_track);
            nadir_view_time:long_name = "Time bin was viewed at nadir view";
            nadir_view_time:units = "seconds";
            nadir_view_time:_FillValue = -999;
            nadir_view_time:valid_min = 0;
            nadir_view_time:valid_max = 86400.999;
        double view_time_offsets(bins_along_track, bins_across_track, number_of_views);
            view_time_offsets:long_name = "Time offsets of views from nadir view";
            view_time_offsets:units = "seconds";
            view_time_offsets:_FillValue = -999;
            view_time_offsets:valid_min = -200;
            view_time_offsets:valid_max = 200;
} // group bin_attributes

group: geolocation_data {
    variables:
        float latitude(bins_along_track, bins_across_track);
            latitude:long_name = "Latitudes of bin locations";
            latitude:units = "degrees_north";
            latitude:_FillValue = -999.f;
            latitude:valid_min = -90.f;
            latitude:valid_max = 90.f;
        float longitude(bins_along_track, bins_across_track);
            longitude:long_name = "Longitudes of bin locations";
            longitude:units = "degrees_east";
            longitude:_FillValue = -999.f;
            longitude:valid_min = -180.f;
            longitude:valid_max = 180.f;
        short altitude(bins_along_track, bins_across_track);
            altitude:long_name = "Altitude at bin locations";
            altitude:units = "meters";
            altitude:_FillValue = -32768s;
            altitude:valid_min = -1000s;
            altitude:valid_max = 10000s;
            altitude:scale_factor = 1.f;
            altitude:add_offset = 0.f;
        short altitude_variability(bins_along_track, bins_across_track);
            altitude_variability:long_name = "RMS variability of altitude at bin locations";
            altitude_variability:units = "meters";
            altitude_variability:_FillValue = -32768s;
            altitude_variability:valid_min = 0s;
            altitude_variability:valid_max = 1000s;
            altitude_variability:scale_factor = 1.f;
            altitude_variability:add_offset = 0.f;
        short sensor_azimuth(bins_along_track, bins_across_track, number_of_views);
            sensor_azimuth:long_name = "Sensor azimuth angles at bin locations";
            sensor_azimuth:units = "degrees from north";
            sensor_azimuth:_FillValue = -32768s;

```

```

        sensor_azimuth:valid_min = -18000s ;
        sensor_azimuth:valid_max = 18000s ;
        sensor_azimuth:scale_factor = 0.01f ;
        sensor_azimuth:add_offset = 0.f ;
short sensor_zenith(bins_along_track, bins_across_track, number_of_views) ;
    sensor_zenith:long_name = "Sensor zenith angles at bin locations" ;
    sensor_zenith:units = "degrees" ;
    sensor_zenith:_FillValue = -32768s ;
    sensor_zenith:valid_min = 0s ;
    sensor_zenith:valid_max = 18000s ;
    sensor_zenith:scale_factor = 0.01f ;
    sensor_zenith:add_offset = 0.f ;
short solar_azimuth(bins_along_track, bins_across_track, number_of_views) ;
    solar_azimuth:long_name = "Solar azimuth angle at bin locations" ;
    solar_azimuth:units = "degrees from north" ;
    solar_azimuth:_FillValue = -32768s ;
    solar_azimuth:valid_min = -18000s ;
    solar_azimuth:valid_max = 18000s ;
    solar_azimuth:scale_factor = 0.01f ;
    solar_azimuth:add_offset = 0.f ;
short solar_zenith(bins_along_track, bins_across_track, number_of_views) ;
    solar_zenith:long_name = "Solar zenith angle at bin locations" ;
    solar_zenith:units = "degrees" ;
    solar_zenith:_FillValue = -32768s ;
    solar_zenith:valid_min = 0s ;
    solar_zenith:valid_max = 18000s ;
    solar_zenith:scale_factor = 0.01f ;
    solar_zenith:add_offset = 0.f ;
short scattering_angle(bins_along_track, bins_across_track, number_of_views) ;
    scattering_angle:long_name = "Scattering angle at bin locations" ;
    scattering_angle:units = "degrees" ;
    scattering_angle:_FillValue = -32768s ;
    scattering_angle:valid_min = 0s ;
    scattering_angle:valid_max = 18000s ;
    scattering_angle:scale_factor = 0.01f ;
    scattering_angle:add_offset = 0.f ;
} // group geolocation_data

group: observation_data {
    variables:
        short obs_per_view(bins_along_track, bins_across_track, number_of_views) ;
            obs_per_view:long_name = "Observations contributing to bin from each view" ;
            obs_per_view:valid_min = 0 ;
            obs_per_view:valid_max = 999 ;
        float QC_bitwise(bins_along_track, bins_across_track, number_of_views, intensity_bands_per_view) ;
            QC_bitwise:long_name = "bitwise quality indicator" ;
            QC_bitwise:units = "unitless" ;
            QC_bitwise:_FillValue = 0.b ;
            QC_bitwise:valid_min = 0.b ;
            QC_bitwise:valid_max = 02^16.b ;
        float QC(bins_along_track, bins_across_track, number_of_views, intensity_bands_per_view) ;
            QC:long_name = "quality indicator" ;
            QC:units = "unitless" ;
            QC:_FillValue = 0.i ;
            QC:valid_min = 0.i ;
            QC:valid_max = 10i ;
        float I(bins_along_track, bins_across_track, number_of_views, intensity_bands_per_view) ;
            I:long_name = "I Stokes vector component" ;
            I:units = "W m^-2 sr^-1 um^-1" ;
            I:_FillValue = -999.f ;
            I:valid_min = 0.f ;

```

```
    I:valid_max = 999.f;
float I_noise(bins_along_track, bins_across_track, number_of_views, intensity_bands_per_view);
    I_noise:long_name = "Random noise of I in bin";
    I_noise:units = "W m^-2 sr^-1 um^-1";
    I_noise:_FillValue = -999.f;
    I_noise:valid_min = 0.f;
    I_noise:valid_max = 800.f;
} // group observation_data
```

## 12 APPENDIX D: SAMPLE CDL FOR SPEXONE

```

netcdf PACE_SPEXone.20220301T123621.L1C.2.6km {
dimensions:
    number_of_views = 5 ;
    intensity_bands_per_view = 400 ;
    polarization_bands_per_view = 50 ;
    bins_along_track = 8000 ;
    bins_across_track = 40 ;

// global attributes:
    :title = "PACE SPEXone Level-1C Data" ;
    :instrument = "SPEXone" ;
    :processing_version = "V1.0" ;
    :Conventions = "CF-1.6" ;
    :institution = "NASA Goddard Space Flight Center, Ocean Biology Processing Group" ;
    :license = "http://science.nasa.gov/earth-science/earth-science-data/data-information-policy/" ;
    :naming_authority = "gov.nasa.gsfc.sci.oceancolor" ;
    :keywords_vocabulary = "NASA Global Change Master Directory (GCMD) Science Keywords" ;
    :stdname_vocabulary = "NetCDF Climate and Forecast (CF) Metadata Convention" ;
    :creator_name = "NASA/GSFC" ;
    :creator_email = "data@oceancolor.gsfc.nasa.gov" ;
    :creator_url = "http://oceancolor.gsfc.nasa.gov" ;
    :project = "PACE Project" ;
    :publisher_name = "NASA/GSFC" ;
    :publisher_email = "data@oceancolor.gsfc.nasa.gov" ;
    :publisher_url = "http://oceancolor.gsfc.nasa.gov" ;
    :processing_level = "L1C" ;
    :cdm_data_type = "swath" ;
    :orbit_number = 12345 ;
    :history = "" ;
    :CDL_version_date = "2020-02-28" ;
    :product_name = "PACE_SPEXone.20220301T123621.L1C.5.2km.nc" ;
    :startDirection = "Descending" ;
    :endDirection = "Ascending" ;
    :time_coverage_start = "2022-03-01T12:36:21Z" ;
    :time_coverage_end = "2022-03-01T13:26:57Z" ;
    :date_created = "2020-03-05T15:12:41Z" ;
    :sun_earth_distance = 0.990849042172323 ;
    :terrain_data_source = "" ;
    :spectral_response_function = "" ;
    :systematic_uncertainty_model = "" ;
    :nadir_bin = 12345 ;
    :bin_size_at_nadir = 2.6km2

group: sensor_views_bands {
variables:
    float view_angles(number_of_views) ;
        view_angles:long_name = "Along-track view angles for sensor" ;
        view_angles:units = "degrees" ;
        view_angles:FillValue = -999.f ;
        view_angles:valid_min = -89. ;
        view_angles:valid_max = 89. ;
    float intensity_wavelengths(number_of_views, intensity_bands_per_view) ;
        intensity_wavelengths:long_name = "Intensity field center wavelengths at each view" ;
        intensity_wavelengths:units = "nm" ;
        intensity_wavelengths:FillValue = -999.f ;
        intensity_wavelengths:valid_min = 320. ;
        intensity_wavelengths:valid_max = 2260. ;
    float intensity_bandpasses(number_of_views, intensity_bands_per_view) ;

```

```

    intensity_bandpasses:long_name = "Intensity field bandpasses at each view" ;
    intensity_bandpasses:units = "nm" ;
    intensity_bandpasses:FillValue = -999.f ;
    intensity_bandpasses:valid_min = 2.5 ;
    intensity_bandpasses:valid_max = 100. ;
float polarization_wavelengths(number_of_views, polarization_bands_per_view) ;
    polarization_wavelengths:long_name = "Polarization field wavelengths at each view" ;
    polarization_wavelengths:units = "nm" ;
    polarization_wavelengths:FillValue = -999.f ;
    polarization_wavelengths:valid_min = 320. ;
    polarization_wavelengths:valid_max = 2260. ;
float polarization_bandpasses(number_of_views, polarization_bands_per_view) ;
    polarization_bandpasses:long_name = "Polarization field bandpasses at each view" ;
    polarization_bandpasses:units = "nm" ;
    polarization_bandpasses:FillValue = -999.f ;
    polarization_bandpasses:valid_min = 2.5 ;
    polarization_bandpasses:valid_max = 100. ;
float intensity_F0(number_of_views, intensity_bands_per_view) ;
    intensity_F0:long_name = "Intensity band solar irradiance" ;
    intensity_F0:units = "W m^-2 μm^-1" ;
    intensity_F0:FillValue = -999.f ;
    intensity_F0:valid_min = 0. ;
    intensity_F0:valid_max = 900. ;
float polarization_F0(number_of_views, polarization_bands_per_view) ;
    polarization_F0:long_name = "Polarization band solar irradiance" ;
    polarization_F0:units = "W m^-2 μm^-1" ;
    polarization_F0:FillValue = -999.f ;
    polarization_F0:valid_min = 0. ;
    polarization_F0:valid_max = 900. ;
} // group sensor_views_bands

group: bin_attributes {
    variables:
        double nadir_view_time(bins_along_track) ;
            nadir_view_time:long_name = "Time bin was viewed at nadir view" ;
            nadir_view_time:units = "seconds" ;
            nadir_view_time:FillValue = -999. ;
            nadir_view_time:valid_min = 0. ;
            nadir_view_time:valid_max = 86400.999 ;
        double view_time_offsets(bins_along_track, bins_across_track, number_of_views) ;
            view_time_offsets:long_name = "Time offsets of views from nadir view" ;
            view_time_offsets:units = "seconds" ;
            view_time_offsets:FillValue = -999. ;
            view_time_offsets:valid_min = -200. ;
            view_time_offsets:valid_max = 200. ;
} // group bin_attributes

group: geolocation_data {
    variables:
        float latitude(bins_along_track, bins_across_track) ;
            latitude:long_name = "Latitudes of bin locations" ;
            latitude:units = "degrees_north" ;
            latitude:FillValue = -999.f ;
            latitude:valid_min = -90.f ;
            latitude:valid_max = 90.f ;
        float longitude(bins_along_track, bins_across_track) ;
            longitude:long_name = "Longitudes of bin locations" ;
            longitude:units = "degrees_east" ;
            longitude:FillValue = -999.f ;
            longitude:valid_min = -180.f ;
            longitude:valid_max = 180.f ;

```

```

short altitude(bins_along_track, bins_across_track) ;
    altitude:long_name = "Altitude at bin locations" ;
    altitude:units = "meters" ;
    altitude:_FillValue = -32768s ;
    altitude:valid_min = -1000s ;
    altitude:valid_max = 10000s ;
    altitude:scale_factor = 1.f ;
    altitude:add_offset = 0.f ;
short altitude_variability(bins_along_track, bins_across_track) ;
    altitude_variability:long_name = "RMS variability of altitude at bin locations" ;
    altitude_variability:units = "meters" ;
    altitude_variability:_FillValue = -32768s ;
    altitude_variability:valid_min = 0s ;
    altitude_variability:valid_max = 1000s ;
    altitude_variability:scale_factor = 1.f ;
    altitude_variability:add_offset = 0.f ;
short sensor_azimuth(bins_along_track, bins_across_track, number_of_views) ;
    sensor_azimuth:long_name = "Sensor azimuth angles at bin locations" ;
    sensor_azimuth:units = "degrees from north" ;
    sensor_azimuth:_FillValue = -32768s ;
    sensor_azimuth:valid_min = -18000s ;
    sensor_azimuth:valid_max = 18000s ;
    sensor_azimuth:scale_factor = 0.01f ;
    sensor_azimuth:add_offset = 0.f ;
short sensor_zenith(bins_along_track, bins_across_track, number_of_views) ;
    sensor_zenith:long_name = "Sensor zenith angles at bin locations" ;
    sensor_zenith:units = "degrees" ;
    sensor_zenith:_FillValue = -32768s ;
    sensor_zenith:valid_min = 0s ;
    sensor_zenith:valid_max = 18000s ;
    sensor_zenith:scale_factor = 0.01f ;
    sensor_zenith:add_offset = 0.f ;
short solar_azimuth(bins_along_track, bins_across_track, number_of_views) ;
    solar_azimuth:long_name = "Solar azimuth angle at bin locations" ;
    solar_azimuth:units = "degrees from north" ;
    solar_azimuth:_FillValue = -32768s ;
    solar_azimuth:valid_min = -18000s ;
    solar_azimuth:valid_max = 18000s ;
    solar_azimuth:scale_factor = 0.01f ;
    solar_azimuth:add_offset = 0.f ;
short solar_zenith(bins_along_track, bins_across_track, number_of_views) ;
    solar_zenith:long_name = "Solar zenith angle at bin locations" ;
    solar_zenith:units = "degrees" ;
    solar_zenith:_FillValue = -32768s ;
    solar_zenith:valid_min = 0s ;
    solar_zenith:valid_max = 18000s ;
    solar_zenith:scale_factor = 0.01f ;
    solar_zenith:add_offset = 0.f ;
short scattering_angle(bins_along_track, bins_across_track, number_of_views) ;
    scattering_angle:long_name = "Scattering angle at bin locations" ;
    scattering_angle:units = "degrees" ;
    scattering_angle:_FillValue = -32768s ;
    scattering_angle:valid_min = 0s ;
    scattering_angle:valid_max = 18000s ;
    scattering_angle:scale_factor = 0.01f ;
    scattering_angle:add_offset = 0.f ;
} // group geolocation_data

group: observation_data {
    variables:
        short obs_per_view(bins_along_track, bins_across_track, number_of_views) ;

```

```

    obs_per_view:long_name = "Observations contributing to bin from each view" ;
    obs_per_view:valid_min = 0 ;
    obs_per_view:valid_max = 999 ;
float QC_bitwise(bins_along_track, bins_across_track, number_of_views, intensity_bands_per_view) ;
    QC_bitwise:long_name = "bitwise quality indicator" ;
    QC_bitwise:units = "unitless" ;
    QC_bitwise:FillValue = 0.b;
    QC_bitwise:valid_min = 0.b;
    QC_bitwise:valid_max = 02^16.b;
float QC(bins_along_track, bins_across_track, number_of_views, intensity_bands_per_view) ;
    QC:long_name = "quality indicator" ;
    QC:units = "unitless" ;
    QC:FillValue = 0.i;
    QC:valid_min = 0.i;
    QC:valid_max = 10i;
float I(bins_along_track, bins_across_track, number_of_views, intensity_bands_per_view) ;
    I:long_name = "I Stokes vector component" ;
    I:units = "W m^-2 sr^-1 um^-1" ;
    I:FillValue = -999.f ;
    I:valid_min = 0.f ;
    I:valid_max = 999.f ;
float I_noise(bins_along_track, bins_across_track, number_of_views, intensity_bands_per_view) ;
    I_noise:long_name = "Random noise of I in bin" ;
    I_noise:units = "W m^-2 sr^-1 um^-1" ;
    I_noise:FillValue = -999.f ;
    I_noise:valid_min = 0.f ;
    I_noise:valid_max = 800.f ;
float QC_polsample_bitwise(bins_along_track, bins_across_track, number_of_views,
polarization_bands_per_view) ;
    QC_bitwise:long_name = "bitwise quality indicator" ;
    QC_bitwise:units = "unitless" ;
    QC_bitwise:FillValue = 0.b;
    QC_bitwise:valid_min = 0.b;
    QC_bitwise:valid_max = 02^16.b;
float QC_polsample(bins_along_track, bins_across_track, number_of_views, polarization_bands_per_view) ;
    QC:long_name = "quality indicator" ;
    QC:units = "unitless" ;
    QC:FillValue = 0.i;
    QC:valid_min = 0.i;
    QC:valid_max = 10i;
float I_polsample(bins_along_track, bins_across_track, number_of_views, polarization_bands_per_view) ;
    I:long_name = "I Stokes vector component at polarimeter spectral sampling" ;
    I:units = "W m^-2 sr^-1 um^-1" ;
    I:FillValue = -999.f ;
    I:valid_min = 0.f ;
    I:valid_max = 999.f ;
float I_polsample_noise(bins_along_track, bins_across_track, number_of_views, polarization_bands_per_view) ;
    I_noise:long_name = "Random noise of I_polsample in bin" ;
    I_noise:units = "W m^-2 sr^-1 um^-1" ;
    I_noise:FillValue = -999.f ;
    I_noise:valid_min = 0.f ;
    I_noise:valid_max = 800.f ;
float Q_over_I(bins_along_track, bins_across_track, number_of_views, polarization_bands_per_view) ;
    Q:long_name = "Q over I (little q) Stokes vector component" ;
    Q:units = "W m^-2 sr^-1 um^-1" ;
    Q:FillValue = -999.f ;
    Q:valid_min = -800.f ;
    Q:valid_max = 800.f ;
float Q_over_I_noise(bins_along_track, bins_across_track, number_of_views, polarization_bands_per_view) ;
    Q_noise:long_name = "Random noise of Q over I in bin" ;
    Q_noise:units = "W m^-2 sr^-1 um^-1" ;

```

```
    Q_noise:_FillValue = -999.f;
    Q_noise:valid_min = 0.f;
    Q_noise:valid_max = 800.f;s
float U_over_I(bins_along_track, bins_across_track, number_of_views, polarization_bands_per_view) ;
    U:long_name = "U over I (little u) Stokes vector component" ;
    U:units = "W m^-2 sr^-1 um^-1" ;
    U:_FillValue = -999.f;
    U:valid_min = -800.f;
    U:valid_max = 800.f;
float U_over_I_noise(bins_along_track, bins_across_track, number_of_views, polarization_bands_per_view) ;
    U_noise:long_name = "Random noise of U in bin" ;
    U_noise:units = "W m^-2 sr^-1 um^-1" ;
    U_noise:_FillValue = -999.f;
    U_noise:valid_min = 0.f;
    U_noise:valid_max = 800.f;
float DOLP(bins_along_track, bins_across_track, number_of_views, polarization_bands_per_view) ;
    DOLP:long_name = "Degree of linear polarization" ;
    DOLP:_FillValue = -999.f;
    DOLP:valid_min = 0.f;
    DOLP:valid_max = 1.f;
float DOLP_noise(bins_along_track, bins_across_track, number_of_views, polarization_bands_per_view) ;
    DOLP_noise:long_name = "Random noise of DOLP in bin" ;
    DOLP_noise:_FillValue = -999.f;
    DOLP_noise:valid_min = 0.f;
    DOLP_noise:valid_max = 1.f;
float AOLP(bins_along_track, bins_across_track, number_of_views, polarization_bands_per_view) ;
    AOLP:long_name = "Angle of linear polarization" ;
    AOLP:units = degrees;
    AOLP:_FillValue = -999.f;
    AOLP:valid_min = 0.f;
    AOLP:valid_max = 360.f;
float AOLP_noise(bins_along_track, bins_across_track, number_of_views, polarization_bands_per_view) ;
    AOLP_noise:long_name = "Random noise of AOLP in bin" ;
    AOLP_noise:units = degrees;
    AOLP_noise:_FillValue = -999.f;
    AOLP_noise:valid_min = 0.f;
    AOLP_noise:valid_max = 360.f;

} // group observation_data
}
```